Wideband tuning of four-wave mixing in solid-core liquid-filled photonic crystal fibers

LORENA VELÁZQUEZ-IBARRA[1,*], ANTONIO DÍEZ[1], ENRIQUE SILVESTRE[2], AND MIGUEL V. ANDRÉS[1]

[1]Departamento de Física Aplicada-ICMUV, Universidad de Valencia, Dr. Moliner 50, 46100, Spain
[2]Departamento de Óptica, Universidad de Valencia, Dr. Moliner 50, 46100, Spain
[*]Corresponding author: lorena.velazquez@uv.es

Compiled May 9, 2016

We present an experimental study of parametric four-wave mixing generation in photonic crystal fibers that have been infiltrated with ethanol. A silica photonic crystal fiber was designed to have the proper dispersion properties after ethanol infiltration for the generation of widely-spaced FWM bands under 1064 nm pumping. We demonstrate that the FWM bands can be tuned in a wide wavelength range through the thermo-optic effect. Band shifts of 175 nm and over 500 nm for the signal and idler bands, respectively, are reported. The reported results can be of interest in many applications, such as CARS microscopy.

OCIS codes: *(060.5295) Photonic crystal fibers; (060.4370) Nonlinear optics, fibers; (190.4380) Nonlinear optics, four-wave mixing.*

http://dx.doi.org/10.1364/ao.XX.XXXXXX

Four-wave mixing (FWM) is a third-order nonlinear parametric process that generates new frequencies, usually called signal and idler, after an intense input field interacts with a nonlinear medium, such as an optical fiber [1]. Photonic crystal fibers (PCFs) offer great flexibility to several FWM applications since they can be fabricated with engineered dispersion profiles to meet specific needs, e.g. in supercontinuum generation [2], wavelength conversion [3] or correlated photon-pair sources [4].

In the last years, the generation of FWM in PCFs has become a suitable option for the implementation of the light source in coherent anti-Stokes Raman scattering (CARS) microscopy systems [5–9]. CARS microscopy has been extensively used [10, 11] in biomedical applications since it allows for imaging of living cells without the need for extrinsic biolabels, with the possibility to obtain high-resolution, real-time in-vivo imaging. CARS requires a light source with quite specific characteristics that, traditionally, have been accomplished using two synchronized solid-state lasers [12] or a laser in conjunction with an optical parametric oscillator (OPO) [13]. Consequently, CARS imaging systems are currently expensive and difficult to operate and, thus, the use of this technique has been restricted mainly to research laboratories. The implementation using PCFs can be a highly valuable contribution that can help to develop robust all-fiber sources for CARS microscopy [5] that would make the technique readily available for medical and biological applications.

Light sources for CARS microscopy based on four-wave mixing in PCFs, use the signal and residual pump of the FWM process as the pump and Stokes signals, respectively, for the CARS process. A limitation currently imposed by this scheme is the difficulty to tune the FWM bands over a wide frequency range without major adjustments, which is desirable in order to cover the vibrational frequencies of different molecules of interest. For example, most Raman band frequencies of biological interest are within the range of (1000-3000) cm^{-1} [14]. Such a wide frequency range would require the capability for tuning the signal wavelength over ∼155 nm in a FWM process pumped at 1064 nm.

Two approaches can be followed to tune the spectral spacing between pump and signal in FWM. Tuning the pump wavelength leads to the shift of signal and idler wavelengths [15]. At a pump wavelength around 1 μm and using typical photonic crystal fibers, in order to cover the frequency range given above, the pump wavelength must be tunable over a few tens of nanometers, which is not easily attainable for simple fiber lasers. The second approach relies on changing the dispersion properties of the PCF dynamically, while the pump wavelength remains unchanged. In this sense, several attempts have been reported. In [16], the effect on the FWM parametric wavelengths of temperature and axial strain applied to a PCF was investigated. A shift of the parametric bands of just a few nanometers was reported, because the dispersion features of the used photonic crystal fibers show little sensitivity to these parameters.

Here, we present an experimental study of FWM frequency tuning through temperature in a liquid-filled photonic crystal fiber. The large thermo-optic coefficient of the used liquid is exploited as a means to induce significant changes in the dispersion profile of the liquid-filled PCF and, hence, in the FWM process. In particular, we used ethanol as the filling liquid because it has a refractive index lower than silica, a large thermo-optic coefficient (almost two orders of magnitude larger than silica), and a relatively low absorption at the wavelengths of interest.

The inset of Figure 1 shows a scanning electron microscope (SEM) image of the fiber used in the experiments. The fiber was designed to have normal dispersion at the experimental pump

wavelength, 1064 nm, when the holes were filled with ethanol. Since the zero dispersion wavelength (ZDW) blue-shifts with lower refractive indices in the cladding, this of course implies that the designed PCF had a ZDW well below 1064 nm before infiltration, and thus it had anomalous dispersion at such pump wavelength. The propagation constant for the fundamental mode, the mode field diameter and the chromatic dispersion were calculated with a fully-vectorial method (FVM) [17]. The wavelength-dependent refractive index of ethanol was taken into consideration in the calculations using the Sellmeier coefficients reported in [18]. FWM parametric wavelengths were obtained by imposing the conservation of energy and momentum. Figure 1 shows the chromatic dispersion of the designed PCF with air in the holes, and with the holes filled with ethanol. The calculated ZDW in the first case was 938 nm, and it shifts to 1098 nm for the ethanol-filled PCF.

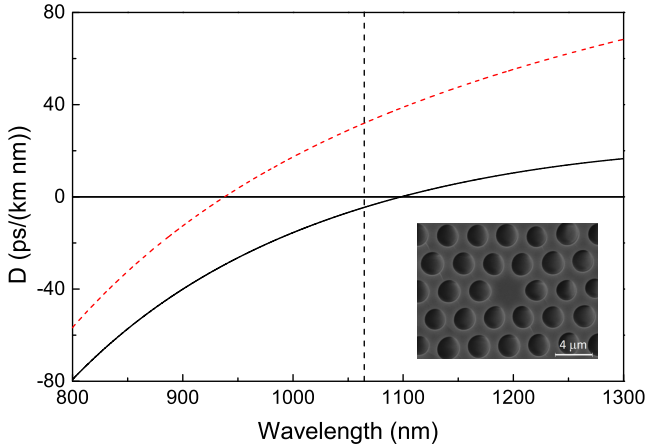

Fig. 1. Chromatic dispersion as a function of wavelength calculated with an FVM for the PCF with air (dashed line) and with ethanol (solid line) at room temperature. The dashed vertical line indicates the experimental pump wavelength.

The PCF was fabricated at the Universidad de Valencia following the stack-and-draw technique. Its geometrical parameters were measured from its SEM image: the pitch is $\Lambda = 3.3\,\mu$m and the hole diameter to pitch ratio is $d/\Lambda = 0.70$. A 75-cm-long section of the fiber was pressure-infiltrated with ethanol, and then it was fusion-spliced to a short section of single-mode fiber (SMF) at the input (injection fiber) and to a multi-mode fiber (MMF) at the output (collection fiber). Thus, the spliced input and output fibers prevent the evaporation of the liquid and enable an easy handling of the PCF. The input fiber needs to be SMF in order to couple power efficiently to the core of the PCF, while the output fiber was chosen to be MMF in order to collect the maximum power, avoiding the losses that PCF-SMF fusion splices usually have. The PCF was pumped with a Nd:YAG Q-switched microchip laser (QSML), which emits 0.72 ns pulses with a repetition rate of 19.9 kHz at 1064 nm. In the experiment, average pump powers between 30 mW and 60 mW were used, measured at the output of the MMF, which correspond to estimated peak powers between 2.1 kW and 4.2 kW.

Figure 2 shows an example of the output spectra of the PCF recorded before and after ethanol infiltration, for pump power levels sufficient to produce nonlinear features. The spectrum corresponding to the air-filled fiber shows the typical closely-spaced sidebands which are characteristic of modulation instability, as it is expected since the fiber is pumped at anomalous dispersion. Instead, the spectrum obtained with the same piece of fiber filled with ethanol shows two widely-spaced bands, centered at 813 nm and 1532 nm, which were produced by degenerate FWM under normal dispersion pumping.

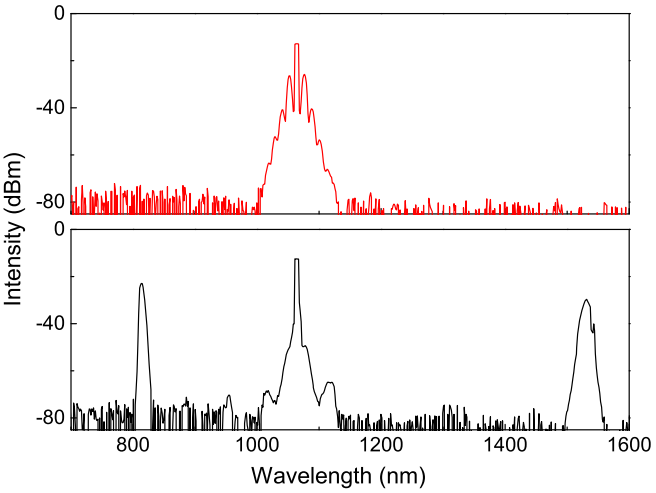

Fig. 2. Output spectra of the PCF before and after infiltration: (top) air, (bottom) ethanol at ΔT=35 °C and 40 mW of pump power.

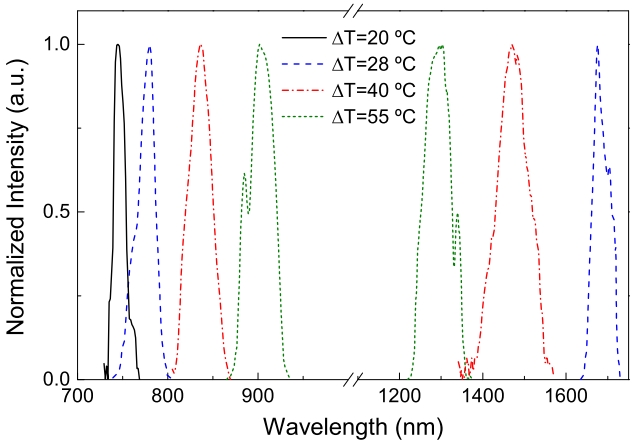

Fig. 3. FWM signal and idler bands obtained at different temperatures

The response of the degenerate FWM process in the ethanol-filled PCF to temperature changes was investigated. The fiber was immersed in a thermal bath to ensure temperature uniformity. Additionally, the temperature of the thermal bath was adjusted in the range between 40 °C and 80 °C, enabling the tuning of the FWM bands. The input and output fibers also allowed the PCF to be completely immersed, ensuring a uniform temperature distribution along its length. Spectra at different temperatures were recorded; the temperature changes, ΔT, were calculated with respect to room temperature. To counteract the changes in the effective mode area that result from the changes in the refractive indices with temperature, the pump power was adjusted in each measurement, by readjusting the

light launching conditions, to keep the amplitude of the FWM bands constant during all measurements.

Figure 3 shows the signal and idler bands for different temperatures. Both bands shift closer to the pump as the temperature raises. Within the investigated temperature change range, from ΔT=20 °C to 60 °C, the signal band shifts from 745 nm to 920 nm, while the idler band shifts from beyond 1750 nm (the limit of the optical spectrum analyzer) to 1260 nm (see Figure 4).

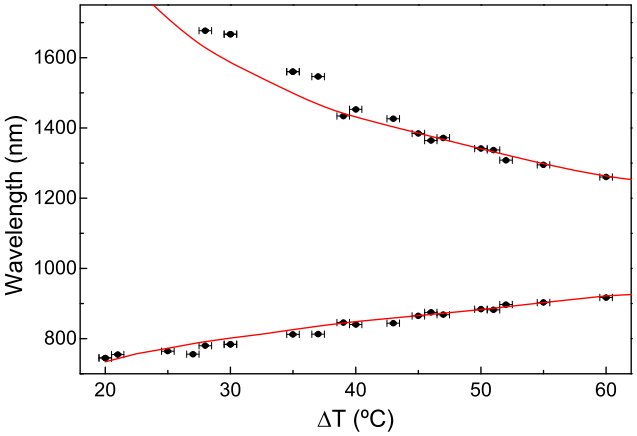

Fig. 4. Experimental (scatter) and calculated (line) signal and idler wavelengths as a function of temperature change in the fiber.

The dependence of the FWM phase-matching wavelengths was investigated also theoretically. We calculated the FWM phase-matching curves for the PCF around 1064 nm at different temperatures. The dependence of the refractive index of ethanol with temperature was considered to be linear, and independent on wavelength. The thermo-optic coefficient (TOC) of ethanol used in the calculations was $-3.99 \times 10^{-4}\ ^{\circ}\mathrm{C}^{-1}$ [19]. The variation of the refractive index of silica with temperature was neglected since its TOC ($8.6 \times 10^{-6}\ ^{\circ}\mathrm{C}^{-1}$ [20]) is two orders of magnitude lower than that of ethanol. Figure 5 (a) shows the theoretical calculation of the zero dispersion wavelength as a function of temperature. The ZDW shifts towards shorter wavelengths as the temperature increases, as it is expected for the negative TOC of ethanol. We found that the shift rate in the ethanol-filled PCF is more than one order of magnitude larger than that in an empty PCF [16]. The dispersion regime changes from normal to anomalous at around ΔT=45 °C, for the experimental pump wavelength.

FWM phase-matching curves for different temperature increments are shown in Figure 5 (b). Signal and idler wavelengths shift towards the pump as the temperature increases. It can be seen that for a temperature change below 20 °C there are no solutions to the phase-matching condition at a pump wavelength of 1064 nm. This is in agreement with what was experimentally observed, since no FWM generation was observed in the PCF at room temperature.

The experimental and numerical parametric wavelengths as a function of temperature change were compared. Numerical simulations that provided the best agreement with the experimental data were obtained for a PCF with $\Lambda = 3.0\,\mu$m and $d/\Lambda = 0.77$ (see Figure 4). These values are quite similar (variation of $\sim 9\,\%$) to the geometric parameters taken from the SEM image of the fabricated PCF. The origin of such differences

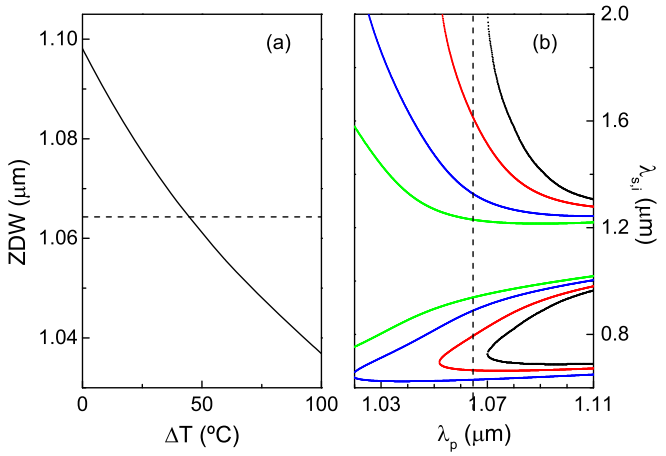

Fig. 5. (a) Theoretical calculation of the ZDW of the ethanol filled PCF as a function of the temperature increment; the horizontal dashed line indicates the pump wavelength. (b) FWM phase-matching curves at different temperatures: ΔT=15 °C (black line), ΔT=30 °C (red line), ΔT=60 °C (blue line) and ΔT=100 °C (green line); the vertical dashed line indicates the pump wavelength. Fiber parameters: $\Lambda = 3.0\,\mu$m, $d/\Lambda = 0.77$.

could be an error in the calibration of the microscope or even a lack of precise knowledge of the material dispersion.

In conclusion, we have experimentally investigated the shift with temperature of widely-spaced FWM parametric bands generated in an ethanol-infiltrated photonic crystal fiber. The signal and idler bands shift towards longer and shorter wavelengths, respectively, with increasing temperature; the achieved shifts for the fiber used in this work are 175 nm for the signal and more than 500 nm for the idler band. Numerical calculations were carried out and show good agreement with the experimental results. The results reported in this work can be implemented together with optical parametric oscillator schemes [21] to achieve a narrowband, highly tunable FWM source for CARS microscopy.

Funding. Ministerio de Economia y Competitividad of Spain and FEDER funds (project TEC2013-46643-C2-1-R), and the Generalitat Valenciana (project PROMETEOII /2014/072) is acknowledged. L. Velazquez also wishes to ackowledge financial support from CONACyT (grant 250888).

REFERENCES

1. G. Agrawal, *Nonlinear Fiber Optics*, Optics and Photonics (Academic Press, 2013), 5th ed.
2. K. M. Hilligsøe, T. V. Andersen, H. N. Paulsen, C. K. Nielsen, K. Mølmer, S. Keiding, R. Kristiansen, K. P. Hansen, and J. J. Larsen, Opt. Express **12**, 1045 (2004).
3. A. Zhang and M. S. Demokan, Opt. Lett. **30**, 2375 (2005).
4. J. Fulconis, O. Alibart, W. J. Wadsworth, P. S. Russell, and J. G. Rarity, Opt. Express **13**, 7572 (2005).
5. M. Baumgartl, M. Chemnitz, C. Jauregui, T. Meyer, B. Dietzek, J. Popp, J. Limpert, and A. Tünnermann, Opt. Express **20**, 4484 (2012).
6. M. Baumgartl, T. Gottschall, J. Abreu-Afonso, A. Díez, T. Meyer, B. Dietzek, M. Rothhardt, J. Popp, J. Limpert, and A. Tünnermann, Opt. Express **20**, 21010 (2012).
7. S. Lefrancois, D. Fu, G. R. Holtom, L. Kong, W. J. Wadsworth, P. Schneider, R. Herda, A. Zach, X. S. Xie, and F. W. Wise, Opt. Lett. **37**, 1652 (2012).

8. E. S. Lamb, S. Lefrancois, M. Ji, W. J. Wadsworth, X. S. Xie, and F. W. Wise, Opt. Lett. **38**, 4154 (2013).
9. T. Gottschall, T. Meyer, M. Baumgartl, B. Dietzek, J. Popp, J. Limpert, and A. Tünnermann, Opt. Express **22**, 21921 (2014).
10. C. L. Evans and X. S. Xie, Annual Review of Analytical Chemistry **1**, 883 (2008).
11. T. Gottschall, T. Meyer, M. Baumgartl, C. Jauregui, M. Schmitt, J. Popp, J. Limpert, and A. Tünnermann, Laser & Photonics Reviews **9**, 435 (2015).
12. J. Cheng, A. Volkmer, L. D. Book, and X. Xie, J. Phys. Chem. B **105**, 1277 (2001).
13. F. Ganikhanov, S. Carrasco, X. S. Xie, M. Katz, W. Seitz, and D. Kopf, Opt. Lett. **31**, 1292 (2006).
14. D. I. Ellis, D. P. Cowcher, L. Ashton, S. O'Hagan, and R. Goodacre, Analyst **138**, 3871 (2013).
15. L. Velazquez-Ibarra, A. Diez, E. Silvestre, M. Andres, M. Martinez, and J. L. Lucio, Phot. Tech. Lett. **23**, 1010 (2011).
16. J. Abreu-Afonso, A. Díez, J. L. Cruz, and M. V. Andrés, Photonics **1**, 404 (2014).
17. E. Silvestre, T. Pinheiro-Ortega, P. Andrés, J. J. Miret, and A. Ortigosa-Blanch, Opt. Lett. **30**, 453 (2005).
18. S. Kedenburg, M. Vieweg, T. Gissibl, and H. Giessen, Opt. Mat. Exp. **2**, 1588 (2012).
19. R. Kamikawachi, I. Abe, A. Paterno, H. Kalinowski, M. Muller, J. Pinto, and J. Fabris, Opt. Comm. **281**, 621 (2008).
20. D. B. Leviton and B. J. Frey, "Temperature-dependent absolute refractive index measurements of synthetic fused silica," Tech. Rep. arXiv:0805.0091, NASA Goddard Space Flight Center (2008).
21. T. Gottschall, T. Meyer, M. Baumgartl, B. Dietzek, J. Popp, J. Limpert, and A. Tünnermann, Opt. Express **22**, 21921 (2014).

FULL REFERENCES

1. G. Agrawal, *Nonlinear Fiber Optics*, Optics and Photonics (Academic Press, 2013), 5th ed.
2. K. M. Hilligsøe, T. V. Andersen, H. N. Paulsen, C. K. Nielsen, K. Mølmer, S. Keiding, R. Kristiansen, K. P. Hansen, and J. J. Larsen, "Supercontinuum generation in a photonic crystal fiber with two zero dispersion wavelengths," Opt. Express **12**, 1045–1054 (2004).
3. A. Zhang and M. S. Demokan, "Broadband wavelength converter based on four-wave mixing in a highly nonlinear photonic crystal fiber," Opt. Lett. **30**, 2375–2377 (2005).
4. J. Fulconis, O. Alibart, W. J. Wadsworth, P. S. Russell, and J. G. Rarity, "High brightness single mode source of correlated photon pairs using a photonic crystal fiber," Opt. Express **13**, 7572–7582 (2005).
5. M. Baumgartl, M. Chemnitz, C. Jauregui, T. Meyer, B. Dietzek, J. Popp, J. Limpert, and A. Tünnermann, "All-fiber laser source for cars microscopy based on fiber optical parametric frequency conversion," Opt. Express **20**, 4484–4493 (2012).
6. M. Baumgartl, T. Gottschall, J. Abreu-Afonso, A. Díez, T. Meyer, B. Dietzek, M. Rothhardt, J. Popp, J. Limpert, and A. Tünnermann, "Alignment-free, all-spliced fiber laser source for cars microscopy based on four-wave-mixing," Opt. Express **20**, 21010–21018 (2012).
7. S. Lefrancois, D. Fu, G. R. Holtom, L. Kong, W. J. Wadsworth, P. Schneider, R. Herda, A. Zach, X. S. Xie, and F. W. Wise, "Fiber four-wave mixing source for coherent anti-stokes raman scattering microscopy," Opt. Lett. **37**, 1652–1654 (2012).
8. E. S. Lamb, S. Lefrancois, M. Ji, W. J. Wadsworth, X. S. Xie, and F. W. Wise, "Fiber optical parametric oscillator for coherent anti-stokes raman scattering microscopy," Opt. Lett. **38**, 4154–4157 (2013).
9. T. Gottschall, T. Meyer, M. Baumgartl, B. Dietzek, J. Popp, J. Limpert, and A. Tünnermann, "Fiber-based optical parametric oscillator for high resolution coherent anti-stokes raman scattering (cars) microscopy," Opt. Express **22**, 21921–21928 (2014).
10. C. L. Evans and X. S. Xie, "Coherent anti-stokes raman scattering microscopy: Chemical imaging for biology and medicine," Annual Review of Analytical Chemistry **1**, 883–909 (2008).
11. T. Gottschall, T. Meyer, M. Baumgartl, C. Jauregui, M. Schmitt, J. Popp, J. Limpert, and A. Tünnermann, "Fiber-based light sources for biomedical applications of coherent anti-stokes raman scattering microscopy," Laser & Photonics Reviews **9**, 435–451 (2015).
12. J. Cheng, A. Volkmer, L. D. Book, and X. Xie, "An epi-detected coherent anti-stokes raman scattering (e-cars) microscope with high spectral resolution and high sensitivity," J. Phys. Chem. B **105**, 1277–1280 (2001).
13. F. Ganikhanov, S. Carrasco, X. S. Xie, M. Katz, W. Seitz, and D. Kopf, "Broadly tunable dual-wavelength light source for coherent anti-stokes raman scattering microscopy," Opt. Lett. **31**, 1292–1294 (2006).
14. D. I. Ellis, D. P. Cowcher, L. Ashton, S. O'Hagan, and R. Goodacre, "Illuminating disease and enlightening biomedicine: Raman spectroscopy as a diagnostic tool," Analyst **138**, 3871–3884 (2013).
15. L. Velazquez-Ibarra, A. Diez, E. Silvestre, M. Andres, M. Martinez, and J. L. Lucio, "Pump power dependence of four-wave mixing parametric wavelengths in normal dispersion photonic crystal fibers," Phot. Tech. Lett. **23**, 1010–1012 (2011).
16. J. Abreu-Afonso, A. Díez, J. L. Cruz, and M. V. Andrés, "Effects of temperature and axial strain on four-wave mixing parametric frequencies in microstructured optical fibers pumped in the normal dispersion regime," Photonics **1**, 404 (2014).
17. E. Silvestre, T. Pinheiro-Ortega, P. Andrés, J. J. Miret, and A. Ortigosa-Blanch, "Analytical evaluation of chromatic dispersion in photonic crystal fibers," Opt. Lett. **30**, 453–455 (2005).
18. S. Kedenburg, M. Vieweg, T. Gissibl, and H. Giessen, "Linear refractive index and absorption measurements of nonlinear optical liquids in the visible and near-infrared spectral region," Opt. Mat. Exp. **2**, 1588–1611 (2012).
19. R. Kamikawachi, I. Abe, A. Paterno, H. Kalinowski, M. Muller, J. Pinto, and J. Fabris, "Determination of thermo-optic coefficient in liquids with fiber bragg grating refractometer," Opt. Comm. **281**, 621–625 (2008).
20. D. B. Leviton and B. J. Frey, "Temperature-dependent absolute refractive index measurements of synthetic fused silica," Tech. Rep. arXiv:0805.0091, NASA Goddard Space Flight Center (2008).
21. T. Gottschall, T. Meyer, M. Baumgartl, B. Dietzek, J. Popp, J. Limpert, and A. Tünnermann, "Fiber-based optical parametric oscillator for high resolution coherent anti-stokes raman scattering (cars) microscopy," Opt. Express **22**, 21921–21928 (2014).